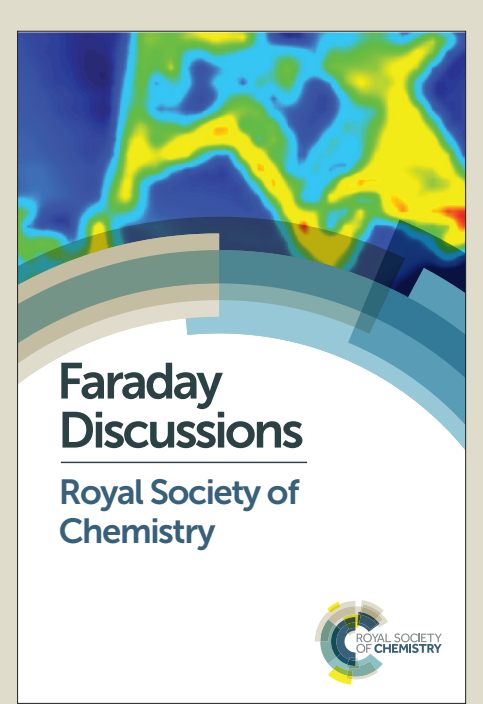
Faraday Discussions

Accepted Manuscript

This manuscript will be presented and discussed at a forthcoming Faraday Discussion meeting. All delegates can contribute to the discussion which will be included in the final volume.

Register now to attend! Full details of all upcoming meetings: http://rsc.li/fd-upcoming-meetings



This is an *Accepted Manuscript*, which has been through the Royal Society of Chemistry peer review process and has been accepted for publication.

Accepted Manuscripts are published online shortly after acceptance, before technical editing, formatting and proof reading. Using this free service, authors can make their results available to the community, in citable form, before we publish the edited article. We will replace this Accepted Manuscript with the edited and formatted Advance Article as soon as it is available.

You can find more information about *Accepted Manuscripts* in the **Information for Authors**.

Please note that technical editing may introduce minor changes to the text and/or graphics, which may alter content. The journal's standard <u>Terms & Conditions</u> and the <u>Ethical guidelines</u> still apply. In no event shall the Royal Society of Chemistry be held responsible for any errors or omissions in this *Accepted Manuscript* or any consequences arising from the use of any information it contains.

This article can be cited before page numbers have been issued, to do this please use: W. Hawkes, D. Huang, P. Reynolds, L. Hammond, M. Ward, N. Gadegaard, J. F. Marshall, T. Iskratch and M. Palma, *Faraday Discuss.*, 2019, DOI: 10.1039/C9FD00023B.



Probing the nanoscale organisation and multivalency of cell surface receptions of cells of cells on the probing the nanoarrays for cellular studies with single-molecule control

William Hawkes, a,b,c ‡ Da Huang,c, ‡ Paul Reynolds,d Linda Hammond,e Matthew Ward,b Nikolaj Gadegaard,d John F. Marshall,e,* Thomas Iskratsch,b,* and Matteo Palma.c,*

- ^a Randall Centre of Cell and Molecular Biophysics, King's College London
- ^b Division of Bioengineering, School of Engineering and Materials Science, Queen Mary University of London
- ^c School of Biological and Chemical Sciences, Queen Mary University of London
- ^d School of Engineering, University of Glasgow
- ^e Centre for Tumour Biology, Barts Cancer Institute, Queen Mary University of London
- ‡ Authors contributed to this work equally
- * Correspondence: j.f.marshall@qmul.ac.uk; t.iskratsch@qmul.ac.uk; m.palma@qmul.ac.uk.

Abstract

Published on 18 March 2019. Downloaded by University College London on 7/8/2019 12:16:10 PM.

Nanoscale organisation of receptor ligands has become an important approach to study the clustering behaviour of cell-surface receptors. Biomimetic substrates fabricated via different nanopatterning strategies have so far been applied to investigate specific integrins and cell types, but without multivalent control. Here we use DNA origami to surpass the limits of current approaches and fabricate nanoarrays to study different cell adhesion processes, with nanoscale spatial resolution and single-molecule control. Notably, DNA nanostructures enable the display of receptor ligands in a highly customisable manner, with modifiable parameters including ligand number, ligand spacing and most importantly, multivalency. To test the adaptability and robustness of the system we combined it with focused ion beam and electron-beam lithography nanopatterning to additionally control the distance between the origami structures (i.e. receptor clusters). Moreover, we demonstrate how the platform can be used to interrogate two different biological questions: 1) the cooperative effect of integrin and growth factor receptor in cancer cell spreading, and 2) the role of integrin clustering in cardiomyocyte adhesion and maturation. Thereby we find previously unknown clustering behaviour of different integrins, further outlining the importance for such customisable platforms for future investigations of specific receptor organisation at the nanoscale.

Introduction

Mammalian cells are embedded in an extracellular matrix (ECM), composed of proteoglycans, glycosaminoglycans and glycoproteins. The ECM components serve as anchoring points for the cells, but binding of integrins and other cell surface receptors also induce cellular signalling cascades which regulate fundamental processes from cell growth, to differentiation, motility or cell death¹. The contact interface between the ECM and cell-binding domains, depends on the receptors' nanoscale spatial organisation^{2, 3} and clustering ⁴⁻⁷. Integrin-ECM interactions are also regulated by cellular (cytoskeletal) and extracellular forces (such as the passive stiffness of the ECM) that affect the stability of the bonds ^{1, 8-10}. Importantly integrin clustering distributes the forces between the receptor-ligand complexes, increasing the maximum force per bond and enabling further integrin adhesion assembly ^{4-6, 9, 11}. Additionally, it is known that integrins work synergistically with other membrane receptors to modulate cell behaviour ^{5, 12-14}.

Different strategies have been developed to fabricate biomimetic substrates for the investigation of ECM geometries in cell spreading and focal adhesion formation $^{6, 15-20}$. Achieving nanoscale control of adhesion receptors, with single molecule resolution, is essential for such investigations; micellar diblock copolymer self-assembly 21 and nanopatterning approaches $^{4, 17, 18, 22}$ have been the most notable strategies to meet this requirement. This has been achieved via the arrangement of metal nanodots in arrays and their use as tethering points for cell-binding domains. These studies demonstrated that in order to establish stable focal adhesions and initiate integrin clusters, the examined cells ($\alpha v \beta 3$ integrin rich fibroblast, osteoblast and cancer cells) require a preferential spacing of ~ 60 nm between single RGD peptides^{3, 4, 6, 15}. However, a recent study with peptidomimetic ligands indicated that major differences exist in the clustering behaviour between $\alpha v \beta 3$ and $\alpha 5 \beta 1$ integrins²³ and information about other integrin subtypes or from different cellular systems is lacking. Most importantly, these strategies have shown only partial application for multivalent investigations with single-molecule control $^{16, 19}$.

In this regard, we recently presented a strategy for the fabrication of biomimetic nanoarrays, based on the use of DNA origami that permit the multivalent investigation of ligand-receptor molecule interactions (simultaneous binding of multiple different ligands) in cancer cell spreading with nanoscale spatial resolution and single-molecule control ²⁰. Here we demonstrate the extension of this approach to different cell adhesion processes. Nanoscale spatial resolution and single-molecule control have been achieved by selectively functionalising DNA nanostructures with specific cell surface receptor ligands for human cutaneous melanoma cells and neonatal rat cardiomyocytes. We combined this with both an electron-beam and focused ion beam nanopatterning approach to assemble DNA Origami in nanoarray configurations. The platforms so developed were then employed for cancer cell spreading investigations and to investigate cardiomyocyte attachment and maturity in response to different peptide configurations. This demonstrates the general applicability and validity of DNA origami nanoarrays as biomimetic substrates for the study of (multivalent) ligand—receptor interactions in the regulation of cellular adhesion and function, with nanoscale spatial resolution and single-molecule control.

Results and Discussion

Published on 18 March 2019. Downloaded by University College London on 7/8/2019 12:16:10 PM.

Design of the arrays and nanostructures

Cellular adhesion to - and probing of - the extracellular environment involves recruitment, activation and clustering of integrins $^{1,\,2,\,11,\,24}$. Sufficient ligand density is key for cell spreading and viability $^{6,\,25,\,26}$. For certain cell types and integrins (especially a $\alpha\nu\beta3$), the preferential ligand spacing required for spreading is 60 nm $^{4,\,15,\,22}$, but a recent study suggested that differences might exist between integrin subtypes 23 . However, the clustering behaviour of integrin subtypes in different cellular systems is still elusive. Furthermore, the role of the nanoscale organisation for the crosstalk between different cell surface receptors is not well understood. To address these challenges, we designed DNA origami nanostructures for two specific applications, namely the investigation of the cooperativity of growth factor and integrin signalling in cancer cells, as well as the role of integrin ligand spacing and densities in the regulation of cardiomyocyte function.

For the cancer cell investigations, DNA origami were engineered and functionalised with A20FMDV2 peptides, selective for $\alpha\nu\beta6$ integrin subtypes, and epidermal growth factor (EGF). The $\alpha\nu\beta6$ integrin subtype is overexpressed in almost one third of carcinomas ²⁷, correlates with poor cancer survival ²⁸ and has been identified as a key marker for metastasis ²⁹ via its modulation of proliferative signalling pathways ³⁰. EGF receptors (EGFR) are known to work cooperatively with integrins and play a key role in regulating the signalling mechanisms at cell adhesion sites ³¹. EGFR is also upregulated in many cancers and together with integrins, regulates cancer cell proliferation, migration and metastasis ³². For this reason, the A20FMDV2 peptides and EGF were chosen for multivalent investigations of cooperative substrate bindings effects of $\alpha\nu\beta6$ integrins

and EGF (respectively) in human melanoma cells (A375P, human malignant cutaneous melanoma cell line). DNA origami were designed to present 6 peptides/EGF along their outer edges, at 60 nm intervals.

To demonstrate the versatility of DNA origami substrate nanopatterning, we sought to extend this approach to the investigation of integrin clustering dynamics for primary neonatal rat cardiomyocytes (NRCs), which due to their contractile nature differ from other cell types in adhesion structure and cytoskeletal organisation 10 , 33 . For this purpose, DNA origami were engineered to present the cyclic RGD (cRGDfC) peptide. Neonatal cardiomyocytes contain relatively high levels of the RGD binding $\alpha 5\beta 1$ integrin subtype which is downregulated shortly after birth (in exchange for laminin binding integrins), but is re-expressed in cardiomyocytes after myocardial infarction and in other cardiac diseases, where it is strongly associated with the activation of pathological signalling pathways 34 . Because of the absence of $\alpha \nu \beta 3$ integrin from NRCs, cRGDfC peptides were utilised to investigate the effect of ligand distance and density on $\alpha 5\beta 1$ integrin clustering and downstream cardiomyocyte behaviour. DNA origami configurations of 6, 12 and 18 peptides were fabricated, constituting inter-peptide spacings of approximately 60 nm, 30 nm and 20 nm (respectively) along the outer edge of each DNA origami structure.

Synthesis and Assembly of Functionalised DNA Origami Nanostructures.

To functionalise DNA origami with A20FMDV2 and cRGDfC, two different attachment chemistries were employed (Figure 1). A20FMDV2 was conjugated to ssDNA via a maleimidethiol reaction, bridging the cysteine thiol on the peptide and a deprotected maleimide on ssDNA (5' end OH group of the phosphate). The cRFDfC peptides were conjugated to ssDNA with a 1 hour, UV mediated thiol-ene reaction³⁵, via a sulfhydryl group on the peptide and a thiol group on ssDNA modified with an acrydite moiety. For all ssDNA-peptide products, Reverse-Phase High Performance Liquid Chromatography (RP-HPLC) was used to verify successful conjugation. Using this approach, the conjugation efficiency was estimated via the relative change in UV adsorption (260 nm) of the unconjugated ssDNA compared to the emerging conjugated product. Additional validation of the yield was obtained using a microvolume spectrophotometer (see methods). The maleimide conjugation approach produced a yield of ~63%, while the acrydite labelling method produced a near 100% yield (Supplementary Figure 1). Purified peptide-ssDNA conjugates were then hybridised to DNA origami in solution via complementary "sticky-end" strands incorporated into the design, enabling selective positioning of peptides on the origami structure with ~6 nm precision.

Individual EGF moieties were selectively positioned and attached to DNA origami via a streptavidin-biotin conjugation technique (Figures 1 and 2). ssDNA was modified to present the biotin which were firstly hybridised to the origami structure. Streptavidin modified EGF was then incubated in solution overnight to achieve successful conjugation to DNA origami structures.

The successful design of both types of DNA nanostructures was further verified by casting diluted solution on muscovite mica substrates. Figure 2 shows atomic force microscopy (AFM) images of the triangular DNA origami employed in this study.

Nanoscale Surface Lithography for Selective Positioning of Functionalised DNA Origami.

Combining nanoscale lithographic substrate fabrication and functionalised DNA origami presents a powerful tool for multivalent investigations into ligand-receptor clustering dynamics. Furthermore, the use of three peptide concentration (6, 12 and 18 peptides) and two DNA origami spacing configurations (200 nm and 300 nm spacing) permits unparalleled control over both local and global peptide concentration and stoichiometry at physiologically relevant sales (30-300 nm). Two approaches were implemented to selectively position individual DNA origami over arrays of up to 3.68 mm² using focussed ion beam (FIB) and electron-beam (EBL) lithography. The first approach implemented was a one-step FIB lithographic process (Figure 3) to fabricate holes in

Faraday Discussions Accepted Manuscrip

metal-coated SiO₂ substrates $^{20, 36}$. Chromium and gold were initially evaporated onto SiO₂ substrates to form 2 nm and 8 nm layers, respectively. Using FIB, 200×200 nm squares were milled into the metal, at 300 nm intervals. A 300 nm spacing per nanoaperture and therefore per DNA origami, was chosen for these nanoarrays to achieve a density of at least 87 ligands persum the exposed SiO₂ was then silanised with a carboxylic acid terminated silane through which origami were covalently cross-linked to the surface using an EDC/sulfo-NHS carbodiimide crosslinking reaction, and the amino modifications in the central void of the origami (Figure 3). The stability of the metallic surface offers a reusable, one-step fabrication of patterned arrays with the ability to selectively position single, functionalised DNA origami, with a yield of 82% \pm 0.17 20 .

The second approach utilised EBL to define the DNA origami bindings sites 37 . Here, 150 nm in diameter holes were patterned in a hexamethyldisilazane layer (1-2 nm thickness) and poly(methyl methacrylate) (~100 nm thickness) resist at intervals of 200 or 300 nm, exposing the underlying SiO₂ (Figure 3). Glass coverslips were patterned with a total of six, 1.5×1.5 mm nano-patterned areas (3 × 200 nm and 3 × 300 nm arrays). An isotropic oxygen plasma etch was then used to generate silanol groups in the holes which were correspondingly silanised with a carboxylic silane. DNA origami were then cross-linked to the surface via the same carbodiimide chemistry as above. While lacking the reusability of the FIB nanopattern, this approach offers the advantages of a higher yield of single DNA origami binding events (100% of sites filled, with ca. 90 % single origami attachment) on transparent substrates.

Multivalent Activation of EGF and ανβ6 Integrins in Human Cutaneous Melanoma Cells

To investigate the synergistic effect of integrin/EGF binding in cancer cell interaction with the ECM, human melanoma cells (A375P) were seeded on FIB nanopatterned substrates functionalised with DNA origami for 1.5 hours before fixation. The cooperative effects of $\alpha v \beta 6$ integrin and EGF binding was evaluated by varying the ratio of A20FMDV2 peptides and EGF ligands (number of peptides:EGF: 1:1, 3:1 and 3:3). The degree of cell attachment and spreading was evaluated with phase contrast and immunofluorescence microscopy. Control experiments of blank FIB nanopatterns did not mediate the attachment of any cells. Melanoma cells adhered to all substrates but the degree of spreading, as indicated by phase images and phalloidin staining, was greater with increasing ligand density (see Figure 4). The EGF receptor (EGFR) sub-family of receptor tyrosine kinases has well validated roles in cancer progression and metastasis³⁸. Immunofluorescence of phosphorylated tyrosines (pTyr) was therefore used as a marker of general tyrosine kinase activity, including EGFR activity. Figure 4 shows that the highly motile melanoma cell line A375Pb6 does not form strong focal adhesions on the origami. Moreover, the ratio of peptide:EGF dramatically changes cell signalling and cell behaviour. At a peptide:EGF ratio of 1:1 the cells are all well spread, actin is distributed diffusely and pTyr signalling is weak. When the ratio is peptide: EGF of 3:1 the cells remain well spread, pTyr signalling increases and some cells show sub membranous actin on one side of the cell, consistent with potential development of a migratory leading edge. Interestingly, additional EGF ligands (peptide:EGF 3:3) reverses the cells to a more rounded phenotype and reduce the pTyr signalling. These data show clearly that nanoscale modulation of ligand density of interactive membrane receptors can induce dramatic changes in cells that warrant more detailed investigations.

Peptide Functionalised DNA Origami Mediates Cell Adhesion and Spreading in Neonatal Rat Cardiomyocytes

To investigate integrin receptor clustering in primary neonatal rat cardiomyocyte (NRC) cultures we first tested the ability of the DNA origami to mediate cell attachment and spreading in a dose dependent manner on random, non-patterned arrays. DNA origami functionalised with 6, 12 and 18 cRGDfC peptides per origami (corresponding to approximate peptide distances of 60, 30, and 20nm, respectively) were cast randomly on 16 mm round glass coverslips and covalently cross-

linked via the EDC/s-NHS carbodiimide chemistry described above. DNA origami without any peptides attached were used as a control. An optimum concentration of 2 nM DNA origami was used to achieve a uniform surface coverage of 10 ± 3 DNA origami/ μ m² (Figure 5). Surfaces were passivated with an methoxy PEG silane and blocked with 5% bovine serum albaminoto minimise non-specific adhesion. NRCs were seeded on the substrates and cultured for 24 hours before the degree of NRC attachment, spreading and phenotype was evaluated. Compared to the 0-peptide control, the number of cells attached to the substrate and the degree of cell spreading increased when 12 or more peptides (30 nm distance between peptides, ~120 \pm 36 ligands/ μ m²) were present on each DNA origami, however cells mainly displayed continuous filamentous instead of striated F-actin staining pattern, indicating an immature phenotype (Figure 5). When 18 peptides were present (180 \pm 54 ligands/ μ m²), a further increase in cell attachment and spreading was observed and sarcomeric striations were clearly visible (see Supplementary Figure 2), thus confirming the ability of functionalised DNA origami to mediate cell attachment and verifying the successful synthesis of the different origami designs.

Nanoscale Control of Global and Local Ligand Clustering Dynamics in Cardiomyocytes

Random positioning of peptide functionalised DNA origami demonstrated that a minimum of 12 peptides per DNA origami (\sim 120 \pm 36 ligands/ μ m²) were required to initiate cardiomyocyte adhesion and spreading. However, random positioning of DNA origami provides no control over ligand geometry above the level of individual origami (~ 85 nm²) and offers limited information on global and local clustering dynamics, which are key for cell adhesion and spreading 5, 21. To investigate this, DNA origami functionalised with 0, 6 or 12 cRGDfC peptides were bound to EBL nanopatterned substrates at 200 nm and 300 nm intervals (Figure 5), and this allowed us to further investigate the role of cluster spacing, due to the differences in receptor clustering behaviour between cardiomyocytes and fibroblasts. EBL nanopatterned substrates were blocked against nonspecific adhesion with a methoxy PEG silane and 5% BSA before seeding NRCs for 24 hours. All cells adhered to the nanopattern were imaged and the degree of cell spreading and cytoskeletal maturity was evaluated by calculating cell area and F-actin intensity. On 0 peptide controls, a small degree of nonspecific cell adhesion was observed (Figure 6), although almost all NRCs were rounded up, presumably in a state of detachment. Negative controls of nanopattern without DNA origami did not facilitate any cardiomyocyte adhesion. Functionalised DNA origami with 6 cRGDfC peptides (60 nm peptide spacing) resulted in the initiation of cell spreading when origami were spaced at 200 nm intervals (150 peptides/μm²), but not at 300 nm intervals (54 peptides/μm²); cell area at 200 nm intervals was measured to be (mean \pm SD) 599 \pm 178 μ m² compared to 442.5 ± 125 µm² at 300 nm intervals, equivalent to the area of rounded unspread cardiomyocytes.

Increasing the number of peptides to 12 per DNA origami (30 nm peptide spacing) resulted in a marked increase in cell attachment and clear initiation of spreading at both 300 nm (108 peptides/ μ m²) and 200 nm (300 peptides/ μ m²) origami spacings, although differences in area, and F-actin content and organisation persisted (Figure 6). At 300 nm, cell area increased to 645 \pm 265 μ m², although a sub-population of rounded cells were still observed. At 200 nm origami spacing, average cell area increased to 755 \pm 192 μ m² and almost all cells were spread, indicating stable adhesion formation.

This difference in spreading and F-actin content (Figure 6) depending on origami distance, while maintaining the same ligand spacing on the origami was surprisingly indicating that in contrast to fibroblasts, the density between the ligands is influencing cardiomyocyte adhesion. 60 nm has been reported to be the optimal spacing to form stable focal adhesions and initiate efficient cell spreading in fibroblasts, osteoblasts and cancer cell lines, which in contrast to NRCs all express high levels of $\alpha v \beta 3$ integrins ^{4, 15, 21, 22, 26}. However, the observed variation in cardiomyocyte spreading at both 200 and 300 nm spacing is indicative of differences in adhesion formation between integrin subtypes in agreement with a previous study using peptidomimetic ligands²³.

View Article Online DOI: 10.1039/C9FD00023B

Our results demonstrate the adaptability of biomimetic nanoarray platforms based on the use of DNA origami to study spreading and adhesion of different cell types. We show that DNA nanostructures conjugated to receptor ligands can be placed with high efficiency and precision onto nanopatterns fabricated with different methods (FIB, EBL). These substrates can then be used to display a wide range of different receptor ligands in a highly controlled manner - alone or in combination with other cell surface receptors. We demonstrate the usefulness of the platform to study different cell types, namely cancer cells and cardiomyocytes. Our findings further show that different receptor types vary strongly in their clustering behaviour; this demonstrates that previous findings from studies employing biomimetic arrays to study RGD/ $\alpha\nu\beta$ 3 integrin interactions at the nanoscale are not universally applicable. Therefore, further work is needed to investigate nanoscale organisation for different receptors and receptor combination in detail. By providing nanoscale spatial resolution, single-molecule control, and multivalent capability, we believe the DNA origami biomimetic nanoarrays presented here are the ideal platform for such studies.

Experimental Methods and Materials Synthesis of DNA Origami.

DNA origami was assembled by combining M13mp18 (5 nM) and staple strands (50 nM) in 50 µL of TAE buffer with 12.5 mM Mg²⁺ (DNA sequences can be obtained at ²⁰). M13mp18 is a bacteria phage vector strand with 7249 bases long. An appropriate quantity of ions, such as magnesium here, or sodium, are required to efficient DNA hybridization. This acts to equilibrate electrostatic repulsion between highly negatively charged DNAs molecules. An amount of 12.5 mM Mg²⁺ sufficient to achieve a high yield of DNA origami and limit any aggregation effects. DNA origami are synthesised by annealing from an initial temperature of 94 °C to completely melt all dsDNA. Temperature step-controlled annealing was carried out in a PCR machine. Samples were cooled from 94 to 65 °Cat a rate of ~0.3 °C per minute. A cooling rate of 0.1 °C per minute is employed from 65 °C to room temperature. The self-assembled DNA origami were then purified using Millipore Amicon Ultra 100 kDa spin columns in a centrifuge at 2000 rcf for 6 min, three times, to remove excess staple strands. DNA origami were adjusted to a concentration ~20 nM and stored in Lo-Bind Eppendorf tubes at 4 °C. A NanoDrop spectrophotometer is used to detect the approximate concentration of DNA origami products based on the constant of a molecular weight of 330 g/mol per base and an extinction coefficient = 33 mg/mL for A260 = the actual result is close to the estimated numbers. To ensure efficient assembly and labelling of DNA origami with peptide conjugates, unmodified staple strands and amino anchors were added at a 5× excess to the M13mp18 backbone and peptide conjugates were added at a 10× excess.

AFM Characterization of DNA Origami.

AFM (Bruker, Dimension Icon) was used to image the DNA origami structures. DNA origami was cast on either silicon dioxide, glass, or mica surfaces for imaging. The DNA origami solution is diluted by TAE buffer with 30 mM MgCl $_2$ to around 1 nM in order to get a good separation of the DNA nanostructures once immobilized on surface. Magnesium is required in the procedure as an ion charged bridge, immobilizing DNA origami to the substrate surfaces. Mica samples were cleaved twice by solid scotch tape immediately prior casting. 5 μ L of diluted DNA origami solution was directly deposited on freshly cleaned mica and left to adsorb on the surface for 2 min. Subsequently, the substrate was washed by distilled water to remove non-adsorbed origami and then blown dry by compressed air. Silicon nitride ScanAsyst-Air tips with 0.4 N/m spring constant

were used to scan the sample by AFM under ScanAsyst Mode. A resolution of 512 pixels per line with 1 Hz scan rate was chosen for appropriate imaging of the DNA nanostructure.

The highly hydrophobic hexamethyldisilazane (HMDS) layer on EBL patterned surfaces made it very difficult to accurately track the surface when scanning in air. Therefore, to characterise DNA origami on the EBL nanopattern, AFM characterisation was carried out in fluid tapping mode. All samples were imaged in 5mM Tris, pH 8.3, 40mM MgCl₂. Silicon nitride ScanAsyst-Fluid+ with 0.7 N/m spring constant were used at a resolution of 512 pixels per line and a 1Hz scan rate. Amplitude setpoint and gain were optimised for each sample and tip.

Modifications of DNA Origami.

Peptide A20FMDV2 was assembled on DNA origami using the maleimide-thiol linkage on ssDNA complementary to sticky-ends. The numbers of peptides on a single origami depends on how many complementary sticky-ends that origami has. Up to 18 positions were chosen in this study (see modified sequences in supplementary information). Commercially available protected maleimide modified ssDNA need to be deprotected before conjugation. 50 nmoles of the protected maleimide modified ssDNA was freeze-dried at first. Deprotection and conjugation will be inefficient in the presence of water. Freeze-dried samples were washed adding 2 mL of anhydrous acetonitrile, and the solvent was evaporated by a rotary evaporator. Two millilitres of anhydrous toluene was added to the vial, mixed, and then evaporated. This rinsing procedure was repeated three times. After the second evaporation, toluene was added and heated to 90 °C for 4 h to deprotect the maleimide modifier. After incubation, the toluene was evaporated. The vial containing the deprotected maleimide-modified ssDNA was immediately mixed with the reduced peptide. The thiol group on the cysteine of the peptide needed to be reduced from the oxide form right before conjugation. The conjugation reaction occurs after the mixing. The mixture was put on a shaker for 1 h to complete the conjugation. Peptide-ssDNA conjugation was validated and purified by reversed-phase HPLC (RP-HPLC) with TEAA buffer (triethyl amine acetic acid). Purified products were freeze-dried and resuspended in TAE buffer. Peptide-ssDNA conjugation was mixed with staple strands and M13mp18, and standard DNA-origami synthesis was carried out. A20FMDV2 is a linear peptide with 21 amino acid. Heating up to 94 °C will not affect the structure and function of this peptide. Epidermal growth factor (EGF) was modified on DNA origami via streptavidin-biotin conjugation. The EGF was biotinylated and assembled with streptavidin which is commercially available. Streptavidin-modified EGF was attached on origami structure via incubation with DNA origami solution which have biotinylated sticky ends. AFM characterization was carried out to confirm the EGF modification.

For cRGDfC peptides, conjugation to ssDNA was performed through UV mediated thiol-ene reaction, via a sulfhydryl group on the peptides and a thiol group on acrydite modified ssDNA (Integrated DNA Technologies). Peptides were diluted to 100 μ M in H₂O containing 100× TCEP pH 7.0, to reduce any disulfide bonds and present the cysteine groups for conjugation. Peptides were then mixed with the acrydite modified ssDNA at a final concentration of 20 μ M and 200 μ M, respectively. Reactions were carried out in 120mM Tris buffer with 11 μ M photoinitiator (2-hydroxy-4'-(2-hydroxyethoxy)-2-methylpropiophenone). Samples were exposed to 260 nm UV light for 1 hour and the conjugates were purified by RP-HPLC and freeze drying, as described above.

Fabrication of FIB and EBL Substrates

Fabrication of the FIB substrates was carried out as previously described 36 . Briefly, Glass coverslips were cleaned in Piranha solution before chromium and gold were evaporated on the surface in 2 nm and 8 nm thick layers (respectively). Substrates were then baked on a hotplate at 300 °C for 15 minutes. 200×200 nm squares were then milled into the substrate using the FIB over

araday Discussions Accepted Manuscrip

an array of a desired size. Prior to cross-linking DNA origami, substrates were cleaned using oxygen plasma for 5 minutes (Harrick, 18W, room air).

Further substrates were produced by direct write EBL on coverslips. Coverslips were solvent cleaned in an ultrasonic bath (acetone followed by methanol, IPA, and water) and dehydrated in a 180C oven overnight. An oxygen plasma treatment for 60s at 100W power prepared the surface for silane deposition, which was done from HMDS vapour in a closed container at 150 C. A 950k molecular weight poly(methyl methacrylate) (PMMA) film was spin coated on the coverslips at 5k rpm, followed by a short solvent bake on a 180C hotplate for 30s. A 10nm aluminium charge conduction layer was evaporated on the coverslips, and they were mounted on a 4-inch silicon wafer for EBL processing using crystalbond 555 adhesive. EBL exposure was carried out as described previously 59 to define arrays of 200nm and 300nm pitch holes, diameter 150nm in the PMMA layer. After exposure, the aluminium charge conduction layer was removed in a 2.6% TMAH solution (MF-CD26) for 30s followed by water rinse. The surface roughness for both kind of patterned surfaces was calculated from AFM topographical heights (Z) by measuring the root mean square $R_q = \sqrt{\frac{\sum Z_t^2}{N}}$ The FIB and EBL substrates exhibited Rq values of , 3.2 ± 0.1 and 0.7 ± 0.1nm respectively.

DNA Origami Patterning and Cross-linking.

For patterning of DNA origami FIB nanofabricated substrates, 60 μL of 1nM of DNA origami were incubated on the surface for 1.5 hours in Tris buffer (5 mM; pH 8.3) with 30 mM MgCl₂. Substrates were placed in a six-well plate with a moist Kimwipe to prevent dewetting and agitated on a shaker. Samples were then washed with Tris buffer (5 mM; pH 8.3) containing 30 mM MgCl₂ A 0.01% solution of carboxyethylsilane (CTES) and incubated for 2 min on a shaker. The buffer was then exchanged for MOPS buffer (10 mM; pH 8.0) with 30 mM MgCl₂). The initial wash with MOPS buffer removed all primary amines from the Tris washes ahead of cross-linking. Next, the MOPS buffer was exchanged with an equal volume of MOPS buffer, pH 8.0, containing 100 mM EDC (1ethyl 3-(3-(dimethylamino)propyl)carbodiimide), and 50 mM sulfo-NHS (Nhydroxysulfosuccinimide). Samples were incubated for 10 minutes at room temperature with gentle agitation. Finally, samples were then washed with the MOPS buffer without MgCl₂ and rinsed with DPBS containing 125 mM NaCl. PBS precipitates with Mg and should remove all non-covalent, physisorbed origami structures. Origami positioning was verified under AFM.

For patterning of DNA origami on e-beam patterned substrates, patterned substrates were first developed in a 2:1 solution of propanol-2:methyl isobutyl ketone for 60 seconds at 23 °C, followed by a 30 seconds wash in 100% propanol-2. DNA origami binding sites were then etched using oxygen plasma treatment (100W, 70 seconds, room air) followed by silanisation with 0.1% CTES in Tris buffer (5 mM, pH 8.0). The PMMA resist was then removed by immersion in NMP at 50 °C and sonicated or 10 minutes. DNA Origami were incubated for 1 hour at room temperature at a concentration of 1 nM in Tris buffer (5 mM, pH 8.3, 50 mM MgCl₂, see supplementary methods for more information on placement conditions). Due to the hydrophobic nature of the HMDS layer and the size of the patterned area, 100 μL of origami solution was required to cover the surface sufficiently. Samples were then washed with MOPS buffer (10 mM, pH 8.1, 50 mM MgCl₂) to remove primary amines, followed by a wash with MOPS buffer (10 mM, pH 8.1, 50 mM MgCl₂) containing 50 mM EDC and 25 mM sulfo-NHS. Finally, samples were then washed with the MOPS buffer without MgCl₂and rinsed with DPBS containing 125 mM NaCl. Before AFM characterisation, samples were placed into deionised H₂O.

Cancer Cell-Spreading Study.

Cells were grown at 37 °C and 8% (v/v) carbon dioxide/air condition in a humidified incubator. Cells were maintained as adherent monolayers on tissue culture plastic. The growth medium contained

DMEM accompanied by 10% FBS. Cells were sub-cultured approximately every 3 days. After incubation with 0.25% (w/v) trypsin/EDTA solution, adhered cells were removed from culture plastic and neutralized by adding three folds of growth medium. Cells were then suspended to fresh tissue culture flasks with fresh growth medium. Cells were removed from tissue culture plastic by trypsin, neutralized, pelleted, and resuspended in fresh growth medium. The substrates were blocked with 1% BSA before cells plating. Growth medium (2 mL) was added to each well and then incubated for 1.5 h. The substrates were carefully washed by PBS twice to remove non-adhered cells. The patterned area with cells was imaged using DIC to observe the cell behaviours. ImageJ was used for counting the cell numbers and average cell area analysis. For this outline of cells were drawn manually after thresholding. The combined cell area were then measured and divided by the cell numbers.

Cardiomyocyte Isolation and Culture

Neonatal rat cardiomyocytes were prepared as previously described ³³. Briefly, newborn rat hearts were dissected into ice-cold ADS buffer (116 mM NaCl, 20mM Hepes, 0.8 mM NaH₂PO₄, 5.6 mM glucose, 5.4 mM KCL, 0.8 mM MgSO₄) and washed once with ADS buffer. The ADS buffer was then removed and hearts were incubated with of 5ml enzyme solution in ADS (ES, 246U collagenase and 0.6 mg pancreatin/mL), for 5 min, at 37 °C under vigorous shaking. Tissues were then triturated with a pipette and the supernatant was discarded. This step was followed by 5-6 digests, until hearts were completely digested. Each time 5ml fresh ES was added to the hearts and incubated 15 min at 37 °C, under shaking. Hearts were pipetted up and down 30 times using a pasteur pipette. The supernatant was then transferred into plating medium (65% DMEM, 17% M199, 10% Horse Serum, 5% FCS, 2% Glutamax, 1% Penecillin/Streptamycin (P/S)). Two digests each were combined in one tube with 20 ml plating medium, then cleared through a 100 mm cell strainer and spun down at 1200 rpm for 5 min at RT, before resuspended in 10 ml plating medium. Cells were pooled together and preplated for 90 min to enrich the cardiomyocytes. Cardiomyocytes were then plated onto the respective substrates in serum free medim (70% DMEM, 22% M199, 5% FCS, 2% Glutamax, 1% Penicillin/ Streptamycin (P/S)). Medium was changed the next day to serum free maintenance medium (78% DMEM, 19% M199, 2% horse serum, 2% Glutamax, 1% P/S).

Immunofluorescence

Immunofluorescent investigations were carried out as described previously³³. Briefly cells were fixed with 4% paraformaldehyde for 10 minutes followed by a wash with PBS. Cells were then permeabilised with 0.2% Triton-X for 5 minutes followed by additional PBS washes. Nonspecific binding was blocked with a 1-hour incubation in 5% BSA before incubation with Alexa 488 labelled phalloidin and DAPI for 1 hour at room temperature to visualise F-actin and cell nuclei, respectively. Substrates were washed with PBS (3 × 5 minutes) and mounted on a coverslip in mowiol mounting medium.

Statistical Analysis

All statistical analysis was carried out using Graphpad Prism 8. For random origami experiments, a one-way ANOVA with Turkey's correction for multiple comparisons was used to test for significant differences. For nanopatterned origami experiments, statistical analyses were carried out using a two-way ANOVA with a Turkey's correction for multiple comparisons.

Conflicts of interest

There are no conflicts to declare.

Acknowledgements

We would like to acknowledge the James Watt Nanofabrication Centre and its staff at the University of Glasgow for the nanofabrication work. WH is recipient of a BBSRC LIDO Studentship DH was supported by the China Scholarship Council. TI was supported by a British Pfeart Foundation Intermediate Basic Science Research Fellowship (FS/14/30/30917) and a BBSRC new investigator award (BB/S001123/1). NG also acknowledges ERC funding through FAKIR 648892 Consolidator Award.

Notes

References

- 1. T. Iskratsch, H. Wolfenson and M. P. Sheetz, *Nat Rev Mol Cell Biol*, 2014, **15**, 825-833.
- 2. K. Zhang, H. Gao, R. Deng and J. Li, *Angew Chem Int Ed*, 2018, **58**, 2-12.
- 3. E. A. Cavalcanti-Adam, T. Volberg, A. Micoulet, H. Kessler, B. Geiger and J. P. Spatz, *Biophys J*, 2007, **92**, 2964-2974.
- 4. M. Schvartzman, M. Palma, J. Sable, J. Abramson, X. Hu, M. P. Sheetz and S. J. Wind, *Nano Lett*, 2011, 11, 1306-1312.
- 5. F. Karimi, A. J. O'Connor, G. G. Qiao and D. E. Heath, Adv Healthc Mater, 2018, 7, e1701324.
- 6. R. Changede, H. Cai, S. Wind and M. Sheetz, bioRxiv, 2018, DOI: 10.1101/435826
- 7. H. Wolfenson, T. Iskratsch and M. P. Sheetz, *Biophys J*, 2014, **107**, 2508-2514.
- 8. J. D. Hood and D. A. Cheresh, *Nat Rev Cancer*, 2002, **2**, 91-100.
- 9. R. Oria, T. Wiegand, J. Escribano, A. Elosegui-Artola, J. J. Uriarte, C. Moreno-Pulido, I. Platzman, P. Delcanale, L. Albertazzi, D. Navajas, X. Trepat, J. M. Garcia-Aznar, E. A. Cavalcanti-Adam and P. Roca-Cusachs, *Nature*, 2017, **552**, 219-224.
- 10. M. Ward and T. Iskratsch, *Biochim Biophys Acta Mol Cell Res*, 2019, DOI: 10.1016/j.bbamcr.2019.01.017.
- 11. P. Roca-Cusachs, T. Iskratsch and M. P. Sheetz, J Cell Sci., 2012, 125, 3025-3038.
- 12. M. Mammen, S. K. Choi and G. M. Whitesides, Angew Chem Int Ed Engl, 1998, 37, 2754-2794.
- 13. J. D. Humphries, A. Byron and M. J. Humphries, *J Cell Sci*, 2006, **119**, 3901-3903.
- 14. M. A. Wozniak, K. Modzelewska, L. Kwong and P. J. Keely, *Biochim Biophys Acta*, 2004, **1692**, 103-119.
- 15. M. Arnold, E. A. Cavalcanti-Adam, R. Glass, J. Blummel, W. Eck, M. Kantlehner, H. Kessler and J. P. Spatz, *Chemphyschem*, 2004, **5**, 383-388.
- 16. H. Cai, D. Depoil, M. Palma, M. P. Sheetz, M. L. Dustin and S. J. Wind, *J Vac Sci Technol B Nanotechnol Microelectron*, 2013, **31**, 6F902.
- 17. H. Cai, J. Muller, D. Depoil, V. Mayya, M. P. Sheetz, M. L. Dustin and S. J. Wind, *Nat Nanotechnol*, 2018, **13**, 610-617.
- 18. Y. Keydar, G. Le Saux, A. Pandey, E. Avishay, N. Bar-Hanin, T. Esti, V. Bhingardive, U. Hadad, A. Porgador and M. Schvartzman, *Nanoscale*, 2018, **10**, 14651-14659.
- 19. G. Le Saux, A. Edri, Y. Keydar, U. Hadad, A. Porgador and M. Schvartzman, *ACS Appl Mater Interfaces*, 2018, **10**, 11486-11494.
- 20. D. Huang, K. Patel, S. Perez-Garrido, J. Marshall and M. Palma, ACS Nano, 2019, 13, 728-736.
- 21. J. Huang, S. V. Grater, F. Corbellini, S. Rinck, E. Bock, R. Kemkemer, H. Kessler, J. Ding and J. P. Spatz, *Nano Lett*, 2009, **9**, 1111-1116.
- 22. M. Schvartzman, K. Nguyen, M. Palma, J. Abramson, J. Sable, J. Hone, M. P. Sheetz and S. J. Wind, *J Vac Sci Technol B Microelectron Nanometer Struct Process Meas Phenom*, 2009, **27**, 61-65.
- 23. V. Schaufler, H. Czichos-Medda, V. Hirschfeld-Warnecken, S. Neubauer, F. Rechenmacher, R. Medda, H. Kessler, B. Geiger, J. P. Spatz and E. A. Cavalcanti-Adam, *Cell Adh Migr*, 2016, **10**, 505-515.
- 24. H. Wolfenson, B. Yang and M. P. Sheetz, *Annu Rev Physiol*, 2019, **81**, 585-605.

- 25. R. Changede, X. Xu, F. Margadant and M. P. Sheetz, *Dev Cell*, 2015, **35**, 614-621.
- 26. R. Zarka, M. B. Horev, T. Volberg, S. Neubauer, H. Kessler, J. P. Spatz and B. Geiger, *Nano Lett*, 2019, DOI: 10.1021/acs.nanolett.8b03513.
- 27. A. Saha, D. Ellison, G. J. Thomas, S. Vallath, S. J. Mather, I. R. Hart and J. F. Marshall, *J. Rathol*, 2010, **222**, 52-63.
- 28. A. L. Wong and S. C. Lee, *Int J Breast Cancer*, 2012, **2012**, 415170.
- 29. Z. Li, S. Biswas, B. Liang, X. Zou, L. Shan, Y. Li, R. Fang and J. Niu, *Sci Rep*, 2016, **6**, 30081.
- 30. Z. Li, P. Lin, C. Gao, C. Peng, S. Liu, H. Gao, B. Wang, J. Wang, J. Niu and W. Niu, *Tumour Biol*, 2016, **37**, 5117-5131.
- 31. N. Balanis, M. Yoshigi, M. K. Wendt, W. P. Schiemann and C. R. Carlin, *Mol Biol Cell*, 2011, 22, 4288-4301.
- 32. J. S. Desgrosellier and D. A. Cheresh, *Nat Rev Cancer*, 2010, **10**, 9-22.
- 33. P. Pandey, W. Hawkes, J. Q. Hu, W. V. Megone, J. Gautrot, N. Anilkumar, M. Zhang, L. Hirvonen, S. Cox, E. Ehler, J. Hone, M. Sheetz and T. Iskratsch, *Developmental Cell*, 2018, 44, 326-336.
- 34. S. Israeli-Rosenberg, A. M. Manso, H. Okada and R. S. Ross, *Circ Res*, 2014, **114**, 572-586.
- 35. J. Torres-Kolbus, C. Chou, J. Liu and A. Deiters, *PLoS One*, 2014, **9**, e105467.
- 36. D. Huang, M. Freeley and M. Palma, *Sci Rep*, 2017, **7**, 45591.
- 37. A. Gopinath and P. W. Rothemund, ACS Nano, 2014, **8**, 12030-12040.
- 38. E. Raymond, S. Faivre and J. P. Armand, *Drugs*, 2000, **60 Suppl 1**, 15-23; discussion 41-12.
- 39. N. Gadegaard, S. Thoms, D. Macintyre, K. Mcghee, J. Gallagher, B. Casey and C. J. M. E. Wilkinson, 2003, 67, 162-168.

Figure Legends:

Published on 18 March 2019. Downloaded by University College London on 7/8/2019 12:16:10 PM

Figure 1: The three linker chemistries used to conjugate ligands to DNA origami. a) Streptavidin-biotin reaction. DNA origami were labelled with biotin and then streptavidin labelled EGF⁰was incubated with labelled origami in solution. b) The first thiol-ene strategy utilised a free thiol on the A20FMDV2 peptide and maleimide modified ssDNA. c) The second thiol-ene strategy utilised a free thiol on the cRGDfC peptide and an acrydite modified ssDNA.

Figure 2: Schematic of functionalised DNA origami: a) DNA origami with peptide and EGF modification. Peptide, EGF and amino anchor modifications were positioned along the inner and outer edges of the DNA origami, and in-plane to the DNA nanostructure; this ensure the availability of the ligands regardless to the orientation of the DNA origami once immobilized on surfaces. b) AFM characterisation of EGF functionalised DNA origami. c) zoom-in AFM image of EGF modified DNA origami. d) Schematic of DNA origami functionalised with 18 cRGDfC Peptides. e) AFM characterisation of peptide modified DNA origami. f) zoom-in AFM characterisation of peptide functionalised DNA origami.

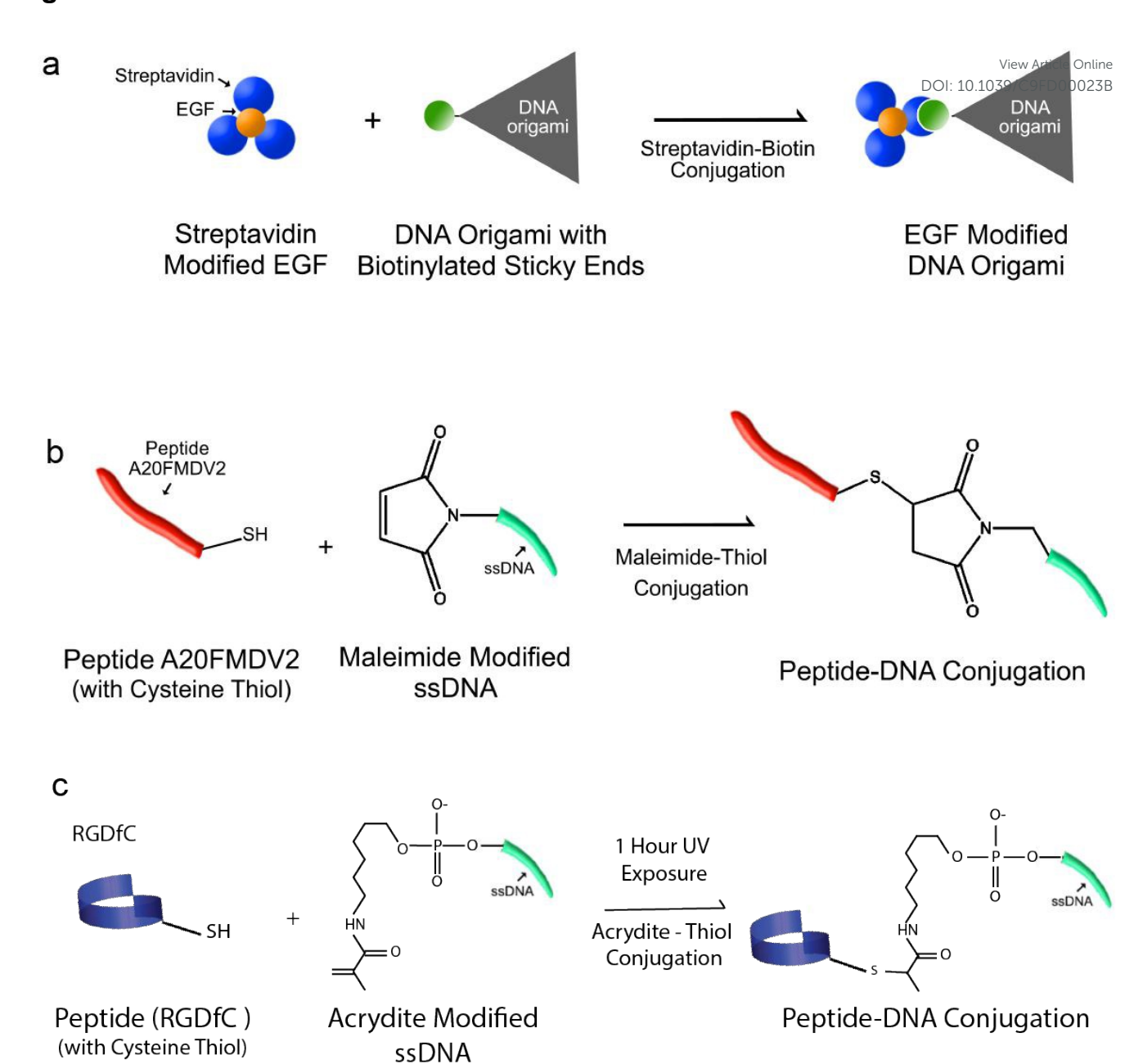
Figure 3: Schematics of FIB: a) and E-beam b) nanopattern fabrication. c) Covalent immobilisation of DNA origami via carbodiimide reaction chemistry between amino modifications on the central void within the DNA origami and carboxylic acid silane. Characterisation of successful cross-linking of origami to the FIB d) and E-beam e) nanopatterns was carried out with AFM.

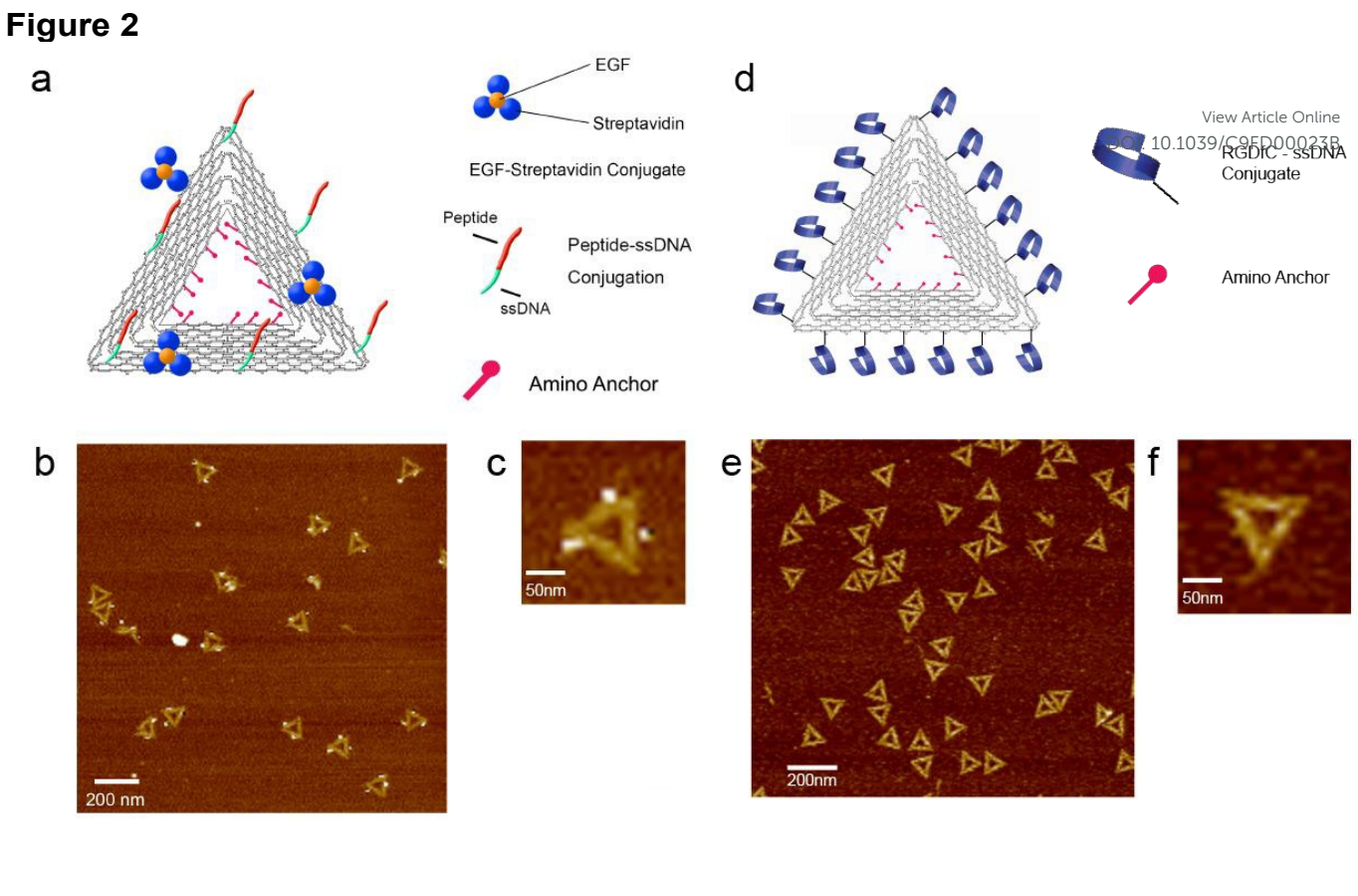
Figure 4: Cancer cell investigation on patterned DNA origami nanoarrays: a) Schematic of cell investigation; b) A375P cell-spreading study on patterned DNA origami substrates with 300 nm spacing include DIC images of cell spreading on different substrates (peptide:EGF=1:1, peptide:EGF=3:1 and peptide:EGF=3:3) with 6× zoom-in inset images, and fluorescent staining images with DAPI (blue), actin (red) and pTyr (green).

Figure 5: Verification of neonatal rat cardiomyocyte (NRC) cell adhesion and spreading mediated by randomly positioned DNA origami functionalised with 0 a), 6 b), 12 c) and 18 d) cRGDfC peptides; this corresponds to peptide distances of 60, 30, and 20nm, respectively. Insets display the DNA origami design used a given condition. N numbers represent the number of cells. f) AFM characterisation of 2nM DNA origami cast randomly on SiO₂ substrates. Fluorescent channels in a-d represent F-actin (green) and DAPI (blue). p values from ANVOA with Tukey correction for multiple comparisons: ***=p<0.001, ****=p<0.0001.

Figure 6: Increasing global and local ligand concentration mediates NRC attachment and spreading. a) AFM images of 200nm and 300nm DNA origami spacing configurations (far left). DAPI (blue) and F-actin (green) staining was used to evaluate cell area b) and integrated F-actin intensity c). p values from ANVOA with Tukey correction for multiple comparisons: ** = p < 0.01, **** = p < 0.001. Box and whisker diagrams: Box limits represent the 25th to 75th percentiles and whiskers represent 1.5× interquartile range. N-numbers represent the number of cells.

Figure 1





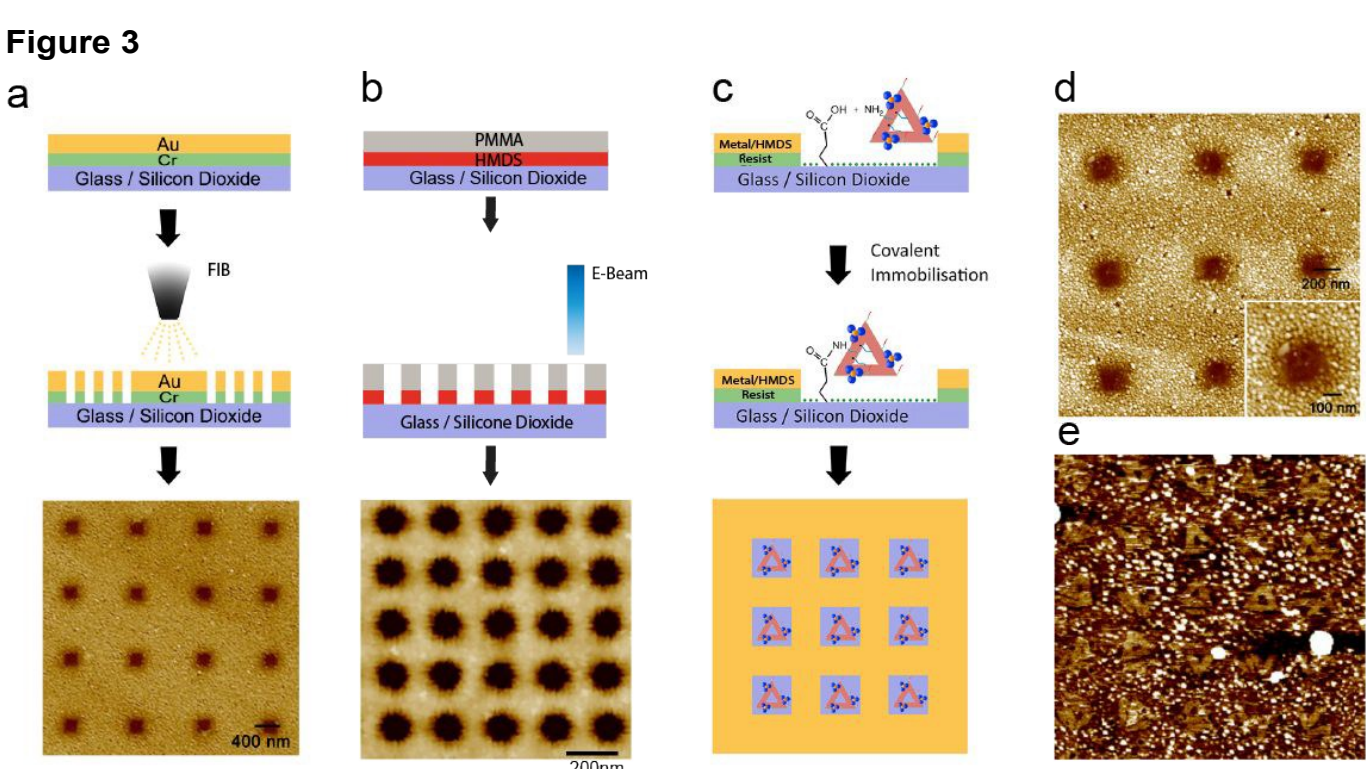
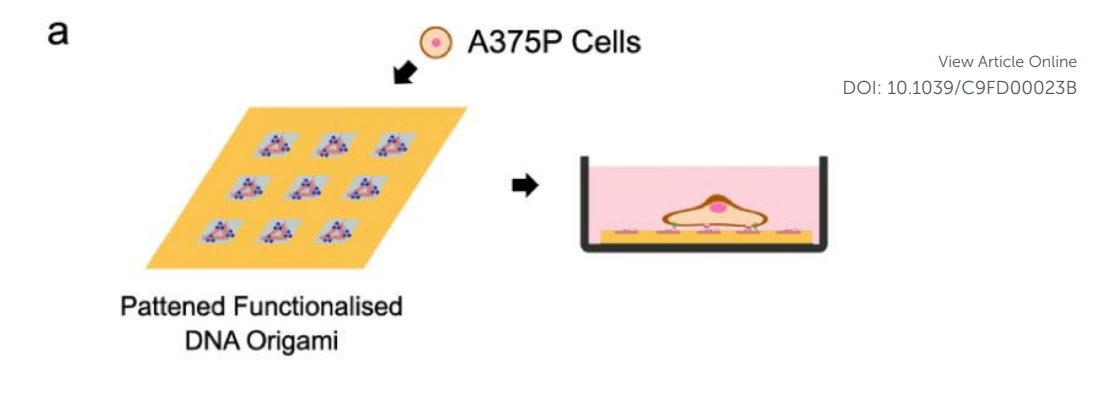
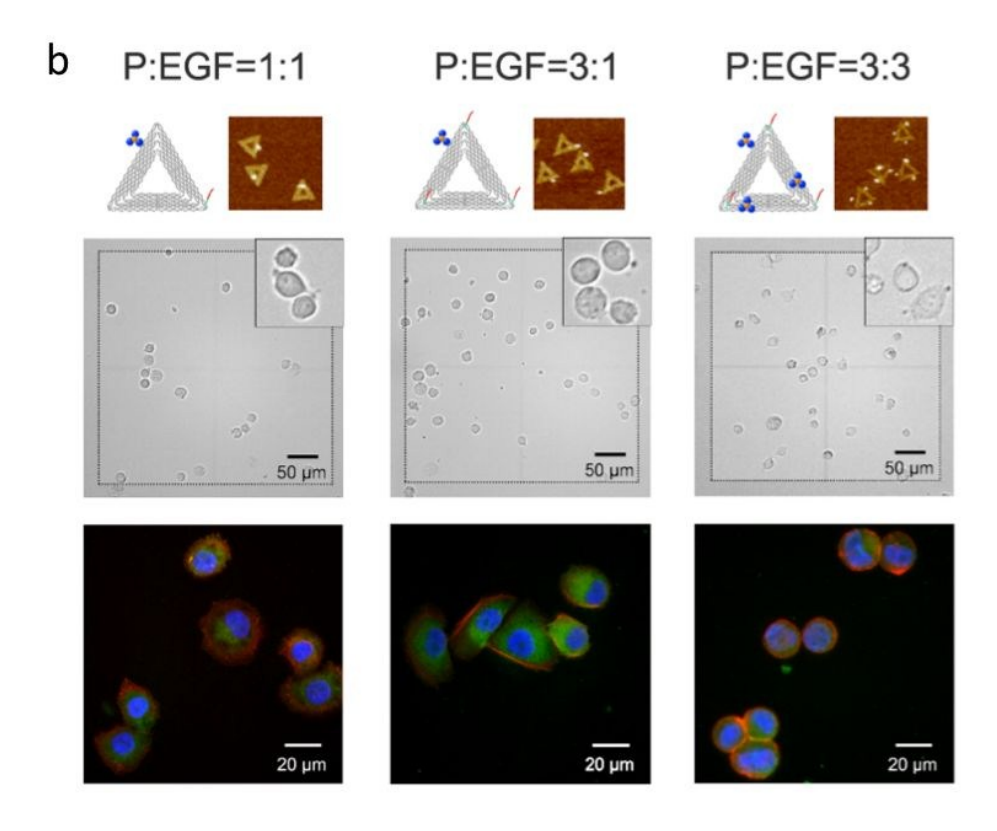
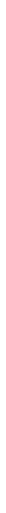
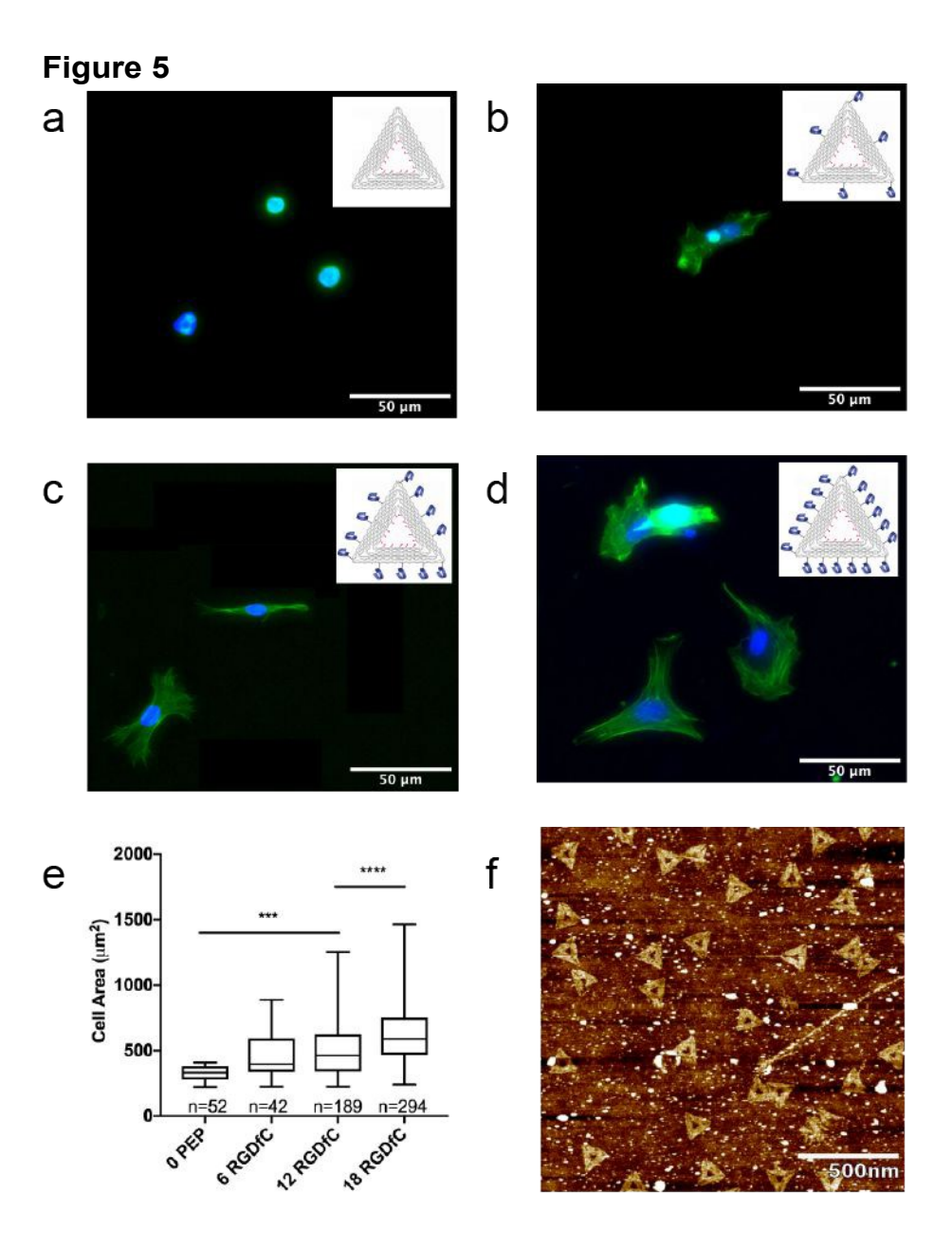


Figure 4



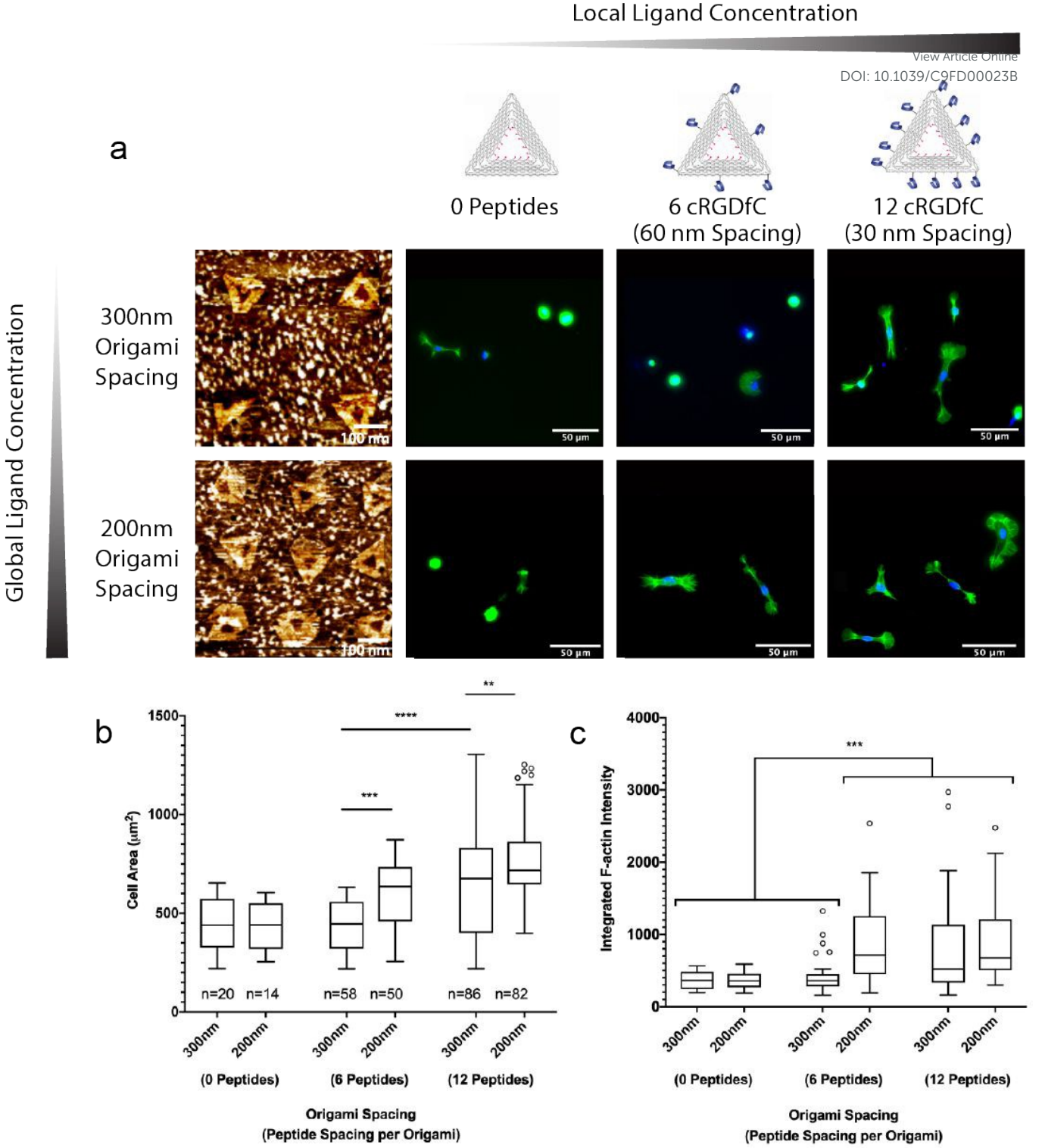






View Article Online DOI: 10.1039/C9FD00023B

Figure 6



DNA Origami nanoarrays with cell surface receptor ligands for cellular studies of human cutaneous melanoma cells and neonatal rat cardiomyocytes. DOI: 10.1039/C9FD00023B

